Principles of slowed hydrogen diffusion through a mucus layer

Owen L. Lewis [*]
Department of Mathematics and Statistics, University of New Mexico, Albuquerque, New Mexico 87131, USA

Ella Missey [†]
Department of Mathematics, Florida State University, Tallahassee, Florida 32306, USA

James P. Keener [‡]
Department of Mathematics, University of Utah, Salt Lake City, Utah 84112, USA

(Received 9 March 2021; accepted 13 September 2021; published 6 October 2021)

The control of transport through mucus layers is a ubiquitous phenomenon in physiological systems. Mucus is often tasked with the mediation of passive, diffusive transport of small ionic species. However, questions remain regarding how mucin gel characteristics (charge density of the polymeric network, binding affinity of ions with mucus) govern the rate at which ions diffuse through mucus layers. Experimental studies measuring hydrogen diffusion through gastric mucus have provided conflicting results, and it is not clear if the rate of ionic diffusion through mucus layers is appreciably different than in aqueous environments (depending on experimental preparation). Here, we present a mathematical analysis of electrodiffussion of two ionic species (hydrogen and chloride) through a mucus layer. In addition to accounting for the chemical binding of hydrogen to the mucus network, we enforce a zero net current condition (as mucus layers in physiological systems are not generally electrogenic) and calculate the Donnan potential that occurs at the edge of the mucus layer. The model predicts the steady-state fluxes of ionic species and the induced potential across the layer. We characterize the dependence of these quantities on the chemical properties of the mucus gel, the composition of the bath solution, and the molecular mobility of the dissolved anion, and we show that the model predictions are consistent with a large portion of the experimental literature. Our analysis predicts that mucus layers generically slow the diffusive transport of hydrogen, but that chemical binding with the network attenuates this effect.

DOI: 10.1103/PhysRevE.104.044403

I. INTRODUCTION

Diffusive transport of ionic species through inhomogeneous gel-like materials is a ubiquitous phenomenon in biology, as well as various engineering contexts. In physiological systems, a common example of such materials are mucus layers. The material known as mucus is a network of glycoproteins called mucins hydrated with water or solvent, and it acts as a selective transport barrier in numerous physiological contexts [1,2]. Mucus layers can be found on many epithelial surfaces, including those in the gastrointestinal tract, respiratory system, and reproductive organs [1,3]. Mucus often serves to control (or prevent) the transport of small ions, nutrients, hormones, or infectious agents, and thus plays a critical role in maintaining healthy physiology [1]. Many of these transport phenomena are passive, and thus governed by diffusion. In addition to contributing to healthy physiology, understanding, and control of diffusive transport across mucus layers is critical to the design of drug delivery systems [2,4].

The barrier properties of gastric mucus in particular have been a subject of debate within mammalian physiology for decades. For more than 70 years, it has been recognized that the layer of gastric mucus adherent to the interior epithelial surface of the stomach segregates the stomach lining from the acidic environment of the gastric lumen (pH $\approx$7 versus pH $\approx$2). This dramatic pH gradient, which is critical for healthy gastric function, is supported across a relatively short length scale (the gastric mucus layer is often $\approx$500 μm thick), causing some to refer to the mucus layer as a "diffusion barrier" [5]. However, it is not at all clear if mucus gels directly inhibit molecular diffusion of ions and other small dissolved species. Indeed, experimental studies attempting to quantify the rate of hydrogen diffusion through mucus (relative to aqueous environments) have produced varied and occasionally contradictory results. Throughout the 1980s and '90s, numerous experiments using Ussing chambers, "flux chambers," or similar devices attempted to measure the diffusive flux of hydrogen ions through a mucus layer separating two ionic baths [6–8]. These experiments report a reduction in hydrogen flux anywhere from 25% to 90% relative to expected values. More recent studies indicate that diffusion of small species is not slowed by mucus gels, and may in fact be promoted by chemical binding interactions with the mucin network [9]. In general, it is still a matter of debate whether electric effects, chemical interactions between

[*]owenlewis@unm.edu
[†]Present address: Department of Chemistry and Biochemistry, Florida State University, Tallahassee, Florida 32306, USA.
[‡]Also at Department of Bioengineering, University of Utah, Salt Lake City, Utah 84112, USA.

hydrogen and mucin, or some other phenomenon plays a dominant role in governing the diffusion of hydrogen through mucus layers.

Numerous theoretical studies have attempted to explain the apparently contradictory data. More broadly, ionic diffusion through charged polymer networks (like mucus) has been the subject of much modeling work. Attempts to modify the diffusion coefficient of small ionic species through polymer networks to account for steric effects date back to the 1950s [10]. Such modifications have more recently been incorporated into polyelectrolyte gel models [11]. However, mucus networks in physiological systems are generally quite sparse, typically ≈97% water by volume, and thus it is unlikely that volume occlusion by the polymeric network plays a significant role in retarding hydrogen transport. Charged polymeric networks have been shown to dramatically slow the diffusion of a single ionic species in molecular dynamics simulations [12]. However, this behavior disappears when a second ion (for example the chloride present in gastric acid) is included. Conversely, classical models of charged resin films have shown that the presence of a larger, "slower" anion (such as chloride), the diffusive flux of a smaller "faster" cation (such as hydrogen) may be reduced [13,14]. Similar behavior has been predicted by more recent models of ion diffusion through hydrogels [15].

Mucus polymers contain several oligosaccharide side chains which may intrinsically (or after being sulphated) exhibit a negative charge and thereby allow the transient binding or association of cations dissolved in the hydrating fluid. The association constants of mucus with several larger cations such as calcium, iron, and cesium have been experimentally measured [16]. Schreiber *et al.* have provided evidence that gastric mucus can bind hydrogen ions in μM concentrations, but did not attempt to ascertain the affinity for mucus and hydrogen binding [17]. To date, few theoretical studies have addressed the impact that hydrogen ions chemically binding to the mucus network may have on ion transport. The work of Marczynski *et al.* has suggested that the ability to form transient bonds with the mucus network may enhance the transport of diffusive species through mucus networks, allowing the species to effectively perform a "sticky" random walk [9]. However, their model incorporates only standard Fickian diffusion, and does not account for the electric potential driven migration which affects small ionic species. Furthermore, few theoretical works account for the Donnan electric potential that occurs at the interface between a charged gel and aqueous solution. It has been shown that this Donnan potential plays a significant role in the behavior of mucus gels [18]. A model of electrodiffusion through a mucus layer which accounts for these electrochemicals effects was developed and analyzed in Ref. [19]. However, that work presupposes the ability to enforce a given electric potential in the baths at either end of the mucus layer, which could necessarily drive a current through the layer. While this may be an accurate representation of *some* experimental apparatuses, it is certainly not an accurate representation of the gastric mucus layer *in vivo*. Furthermore, few of the extant experimental studies attempted to control the electric potential across the layer through which ion diffusion was measured [6,7].

In this work, we analyze a Nernst-Planck-like model of electrodiffusion of a cation/anion through a charged, chemically active mucus layer. This model is similar to that analyzed in Ref. [19], and is an attempt to recapitulate as simply as possible flux chamber experiments such as those in Refs. [7,8]. We explicitly account for binding and unbinding between the cation and the gel network, as well as the Donnan equilibrium potential at the gel and bath interface. In place of boundary conditions on the electric potential, we impose a zero current condition on the full system. The steady-state flux of hydrogen across the gel layer is quantified as a function of parameters which describe the electrochemical nature of the gel layer, as well as the relative mobilities of the cation-anion pair. This flux is then compared to the "expected flux" of standard electrodiffusion in an aqueous environment. Generically, we show that the transport of hydrogen is slowed by the presence of the mucus gel, and that this effect is reduced by chemical binding of hydrogen to the gel. In multiple limiting cases, the model predicts zero transport and recapitulates the classical Nernst potential across a semipermeable membrane. Perhaps most importantly, we show that the observed flux of hydrogen depends nonlinearly on the bath concentrations, which may explain the apparent contradiction in experimental studies which compare it to the "expected flux" which depends linearly on bath concentrations.

II. MATHEMATICAL MODEL

In this work we analyze the behavior of a minimal model of hydrogen diffusion through a mucuslike layer put forth in Ref. [19]. The model describes the transport of a single cationic-anionic species pair through a domain containing a fixed, charged material (mucus polymeric network) that the cation may bind to. The extent of the domain is described by a single spatial variable $0 \leqslant X \leqslant L$. The state variables consist of four quantities: the concentration of the cation (hydrogen) dissolved in fluid, the concentration of dissolved anion (chloride), the concentration of cation bound to the background network (denoted $H(x,t)$, $C(x,t)$, and $B(x,t)$, respectively), and the electric potential Ψ. In the limit that the background material occupies zero volume (i.e., a sparse network), the transport of dissolved ion concentrations may be described by the Nernst-Planck equation, modified with reaction terms that describe binding and unbinding with the background material via mass action kinetics. It is assumed that bound cations are fixed to the immobile network, but may change due to binding and unbinding reaction. Finally, we assume electroneutrality. The partial differential equations describing these dynamics are

$$H_t = \frac{\partial}{\partial X}\left(D_H \frac{\partial H}{\partial X} + D_H H \frac{\partial \Psi}{\partial X}\right) - k_+ H(C_T - B) + k_- B, \tag{1}$$

$$C_t = \frac{\partial}{\partial X}\left(D_C \frac{\partial C}{\partial X} - D_C C \frac{\partial \Psi}{\partial X}\right), \tag{2}$$

$$B_t = k_+ H(C_T - B) - k_- B, \tag{3}$$

$$H - C - (C_T - B) = 0. \tag{4}$$

Here, Ψ is measured in nondimensional "thermal voltage" (which may be converted to standard voltage by multiplying by RT/F, where R is the ideal gas constant, T is absolute temperature, and F is the Faraday constant). The diffusivity of each ion j is denoted D_j, C_T is the concentration of binding sites on the background media, and k_+ and k_- are the rates for hydrogen and background binding and unbinding, respectively. It is assumed that binding sites and negative charge on the background material exist in a one-to-one correspondence. It is also assumed that the charge density of the mucus network is uniform throughout the layer and independent of ionic concentrations. Thus, our model ignores the possible swelling and condensation of the mucus network in response to the ionic composition of the bath [18,20]. While mucus networks are known to change volume dramatically in response to concentration of divalent salts (such as calcium chloride), monovalent ionic solutions (like hydrogen chloride) typically cause volume changes of no more than 12%. Thus, we assume that the background network volume (and therefore density) is a constant.

Equations (1) and (2) are subject to Dirichlet boundary conditions, which are discussed in more detail in Sec. II B. For now, we envision the domain of interest being placed between two baths of hydrogen chloride solution of known concentrations (which satisfy electroneutrality). The concentration for both dissolved species is $\mathscr{B}_0$ and $\mathscr{B}_1$ in the left and right baths, respectively. We assume that both baths are large enough that flux of ions through the interior domain does not alter these concentrations appreciably. Finally, no boundary conditions are specified for the electric potential Ψ, which represents a major difference between this analysis and previous work [19]. In Ref. [19] Dirichlet conditions were imposed on Ψ to mimic experiments performed using Ussing chamberlike devices where the potential drop between baths can be controlled. The imposed boundary conditions were integral to the results of that analysis. However, in other experimental preparations such as [7] and the gastric mucus layer *in vivo*, there is no mechanism to impose the electric potential or electric field. Furthermore, most of the relevant ion transport mechanisms across the epithelial cell surface (at the edge of the mucus layer) are either passive or nonelectrogenic (hydrogen and potassium exchange, hydrogen and sodium exchange, etc.) and therefore not drive a net current [26]. Therefore, in this work, we assume that at steady state, the flux cations and anions must result in zero DC current. This condition is discussed more below.

We are interested in the steady-state flow of ions through the domain, and thus assume that all time derivatives are zero. In this case, Eq. (3) may be used to eliminate the reaction terms from Eq. (1). Eqs. (1) and (2) may then be integrated in space to arrive at the following system that describes the steady-state distribution of ions and the electric potential:

$$D_H\frac{dH}{dX}+D_HH\frac{d\Psi}{dX}=-J_H, \tag{5}$$

$$D_C\frac{dC}{dX}-D_CC\frac{d\Psi}{dX}=-J_C, \tag{6}$$

$$0=\mathscr{K}H(C_T-B)-B, \tag{7}$$

$$H-C+B-C_T=0. \tag{8}$$

Here, $\mathscr{K}=k_+/k_-$ is the association constant of the binding reaction. J_H and J_C are the (as yet unknown) steady-state fluxes of hydrogen and chloride through the domain, which are constant. The minus sign in front of J_H and J_C is used so positive fluxes correspond with transport from left to right. Zero net current condition is written as

$$J_H=J_C. \tag{9}$$

Equations (5)–(9) represent the system that we analyze, and quantifying the dependence of J_H on parameters represents a major goal of this analysis.

A. Nondimensionalization

To nondimensionalize Eqs. (5)–(8) we choose the domain length (L) as a length scale, and the left bath concentration ($\mathscr{B}_0$), which is assume to be nonzero, as the characteristic concentration. As a scale for the ionic fluxes, we utilize the characteristic Fickian flux of that particular ion ($D_H\mathscr{B}_0/L$ and $D_C\mathscr{B}_0/L$, respectively). This leads to the following nondimensional quantities (we use the convention that lower case roman letters indicate nondimensional variables):

$$\begin{gathered}h=\tfrac{H}{\mathscr{B}_0},\quad c=\tfrac{C}{\mathscr{B}_0},\quad b=\tfrac{B}{\mathscr{B}_0},\\ j_h=\tfrac{J_HL}{D_H\mathscr{B}_0},\quad j_c=\tfrac{J_CL}{D_C\mathscr{B}_0},\quad x=\tfrac{X}{L}.\end{gathered} \tag{10}$$

The electric potential remains unchanged, as it is already nondimensional. Upon rescaling, Eqs. (5)– (9) become

$$\frac{dh}{dx}+h\frac{d\Psi}{dx}=-j_h, \tag{11}$$

$$\frac{dc}{dx}-c\frac{d\Psi}{dx}=-j_c, \tag{12}$$

$$0=Kh(c_T-b)-b, \tag{13}$$

$$h-c-(c_T-b)=0, \tag{14}$$

$$j_c=\alpha j_h. \tag{15}$$

Here, $K=\mathscr{K}\mathscr{B}_0$ is the nondimensional association constant of the binding reaction, $c_T=C_T/\mathscr{B}_0$ is the nondimensional density of binding sites on the background network, and $\alpha=D_h/D_C$ is the ratio of ionic diffusion coefficients.

B. Boundary data

We envision baths of known ionic composition exist at either end of the mucus layer which defines our domain. It is known that electric double layers may form at the interface between gel and bath for polyelectrolyte materials such as mucus. However, the length scale of these double layers is comparable to the Debye length [21], which is typically several orders of magnitude smaller than the gel layer itself. Away from the interface, electroneutrality holds in both the gel and the bath. Therefore, our model does not explicitly resolve the double layers at the boundary. Instead, we account for the apparent discontinuity (on the length scales of interest) in model variables across the gel/bath interface. An interface condition must be satisfied that relates the bath conditions to the boundary values for Eqs. (11) and (12) (which we refer to

as the "inner problem"). We denote boundary values for the inner problem (superscript "in") using the following notation:

$$h_0^{\text{in}} = \lim_{x\to 0+} h(x), \quad h_1^{\text{in}} = \lim_{x\to 1-} h(x), \tag{16}$$

$$c_0^{\text{in}} = \lim_{x\to 0+} c(x), \quad c_1^{\text{in}} = \lim_{x\to 1-} c(x), \tag{17}$$

$$\Psi_0^{\text{in}} = \lim_{x\to 0+} \Psi(x), \quad \Psi_1^{\text{in}} = \lim_{x\to 1-} \Psi(x). \tag{18}$$

Similarly, we represent the nondimensional bath conditions (superscript "out") using the following notation:

$$h_0^{\text{out}} = \mathscr{h}_0 = 1, \quad h_1^{\text{out}} = \mathscr{h}_1, \tag{19}$$

$$c_0^{\text{out}} = \mathscr{h}_0 = 1, \quad c_1^{\text{out}} = \mathscr{h}_1, \tag{20}$$

$$\Psi_0^{\text{out}} = 0, \quad \Psi_1^{\text{out}} = \Psi_1. \tag{21}$$

Because we scaled concentrations using the left bath concentration ($\mathscr{B}_0$), we may assume that $\mathscr{h}_0 = 1$, and without loss of generality we define the left bath potential to be zero.

The appropriate interface condition is given by the so-called Donnan equilibrium potential [22]. The ion concentrations and potential jump across the interface must satisfy

$$\Psi_j^{\text{in}} - \Psi_j^{\text{out}} = \ln\left(\frac{h_j^{\text{out}}}{h_j^{\text{in}}}\right) = -\ln\left(\frac{c_j^{\text{out}}}{c_j^{\text{in}}}\right), \tag{22}$$

at each interface ($j = 0, 1$). Some models used to analyze the swelling behavior of polyelectrolyte gels such as mucus explicitly account for changes in gel volume in the Donnan equilibrium potential [21,23]. However, we again assume that the background network does not undergo appreciable changes in volume due to ionic concentrations, and therefore the Donnan potential has the form given here. Suitable algebraic manipulation (see Supplemental Material [24]) yields the interior hydrogen concentration at the interface (h_j^{in}) defined implicitly as the (unique positive) solution to the cubic polynomial equation

$$P(u) = Ku^3 + u^2 - \left(c_T + K\mathscr{h}_j^2\right)u - \mathscr{h}_j^2 = 0. \tag{23}$$

In the degenerate case that $K = 0$ and/or $c_T = 0$, a lower order polynomial equation must be solved for the inner concentration, but it can be shown that there is still a unique positive solution h_j^{in}.

C. Solution

After algebraic manipulation of Eqs. (11)–(15) (see Supplemental Material [24]), we arrive at a separable differential equation for the hydrogen concentration:

$$\frac{dh}{dx} = f(h) := \frac{\left[(1+\alpha)j_h K h^2 + (1+\alpha)j_h h - c_T j_h\right](Kh+1)}{-2K^2h^3 - 4Kh^2 - 2h + c_T}. \tag{24}$$

Integration of Eq. 24 yields the implicit relationship between h and x,

$$\frac{1}{j_h}\left(\mathscr{F}(h; c_T, K, \alpha) - \mathscr{F}\left(h_0^{\text{in}}; c_T, K, \alpha\right)\right) = \int_{h_0^{\text{in}}}^{h} \frac{1}{f(u)}\,du = \int_0^x du = x, \tag{25}$$

where h_0^{in} is the hydrogen concentration at the left boundary of the "inner" domain. The semicolon is meant to delineate functional dependence on state variables from dependence on parameters. The function $\mathscr{F}$ has the form

$$\begin{aligned}\mathscr{F}(u; c_T, K, \alpha) = {} & \frac{4Kc_T + \alpha^2 + 2\alpha + 1}{K(\alpha+1)\sqrt{(\alpha+1)(4Kc_T + \alpha + 1)}} \tanh^{-1}\left[\frac{(\alpha+1)(2Ku+1)}{\sqrt{(\alpha+1)(4Kc_T+\alpha+1)}}\right] \\ & + \frac{1}{2K}\ln\left|-K(\alpha+1)u^2 - (\alpha+1)u + c_T\right| - \frac{1}{K}\ln|Ku+1| - \frac{2}{(\alpha+1)}u.\end{aligned} \tag{26}$$

An associated differential equation for Ψ as a function of h may be derived (see Supplemental Material [24]). Solving this differential equation gives

$$\Psi(h) = \mathscr{G}(h; c_T, K, \alpha) - \mathscr{G}\left(h_0^{\text{in}}; c_T, K, \alpha\right) + \Psi_0^{\text{in}}, \tag{27}$$

where

$$\mathscr{G}(h; c_T, K, \alpha) - \mathscr{G}\left(h_0^{\text{in}}; c_T, K, \alpha\right) = \int_{h_0^{\text{in}}}^{h} \frac{-j_h + f(u)}{uf(u)}\,du. \tag{28}$$

$$\begin{aligned}\mathscr{G}(u; c_T, K, \alpha) = {} & \frac{2\alpha}{\sqrt{(\alpha+1)(4Kc_T+\alpha+1)}} \tanh^{-1}\left[\frac{(\alpha+1)(2Ku+1)}{\sqrt{(\alpha+1)(4Kc_T+\alpha+1)}}\right] \\ & + \frac{1}{(\alpha+1)}\ln\left|-K(\alpha+1)u^2 - (\alpha+1)u + c_T\right| - \ln\left|Ku+1\right|.\end{aligned} \tag{29}$$

D. Determining fluxes

Solution to the full system proceeds in the following manner:

(1) Given parameters within the domain which characterize the electrochemical nature of the background material (K and c_T), as well as the two ions in question (α) and the

bath concentrations ($\mathscr{C}_j$), we can solve Eq. (23) for the inner concentration of hydrogen at each interface (h_j^{in}).

(2) Once boundary data for the inner hydrogen profile are known, Dirichlet boundary conditions on Eq. (25) imply

$$\mathscr{F}\left(h_1^{\text{in}}; c_T, K, \alpha\right) - \mathscr{F}\left(h_0^{\text{in}}; c_T, K, \alpha\right) = j_h, \tag{30}$$

where all parameters on the left hand side are known. This allows us to evaluate the flux j_h.

(3) Upon determining j_h, we can evaluate Eqs. (25) and (27) to determine the hydrogen concentration and electric potential (implicitly) within the domain.

(4) Finally, after determining the electric potential within the domain, Eq. (22) is used to evaluate the electric potential in the right bath (Ψ_1^{out}), which is the potential drop from bath to bath.

III. RESULTS

A. No mucus

When $c_T = 0$ (regardless of the value of K), the model represents a network that exhibits no binding sites or charge density. In this case, solving the Donnan problem yields that the hydrogen concentration at the boundary of the inner domain is equal to that within the bath (as is the electric potential)

$$h_0^{\text{in}} = \mathscr{C}_0, \quad h_1^{\text{in}} = \mathscr{C}_1 \quad \Psi_0^{\text{in}} = \Psi_0^{\text{out}} = 0, \quad \Psi_1^{\text{in}} = \Psi_1^{\text{out}}. \tag{31}$$

Furthermore, rederivation of the function $\mathscr{F}$ gives a particularly simple form

$$\mathscr{F}(h;\alpha) = \frac{-2h}{(\alpha+1)}. \tag{32}$$

Rederivation of $\mathscr{G}$ yields

$$\mathscr{G}(h;\alpha) = \frac{-\ln(h)(\alpha-1)}{(\alpha+1)}. \tag{33}$$

Equation (32) implies that the flux of hydrogen through the domain is given by

$$j_h = \frac{2}{(\alpha+1)}(\mathscr{C}_0 - \mathscr{C}_1) = \overline{j_h}. \tag{34}$$

Thus, flux is proportional to the difference in bath concentration, exactly as one would expect in aqueous diffusion. We introduce the notation $\overline{j_h}$ here to denote the flux of hydrogen in the presence of no mucus. In later sections it will be convenient to compare calculated values of j_h to this nominal value. We note here that in the limit that the anion mobility is much less than that of hydrogen ($\alpha \to \infty$), the flux of hydrogen approaches zero, as the zero current condition will not allow the transport of cations without corresponding flux of anions. Alternately, in the limit that the anion has much larger mobility,

$$\lim_{\alpha\to 0} j_h = 2(\mathscr{C}_0 - \mathscr{C}_1), \tag{35}$$

which is precisely twice the flux one would expect due to standard Fickian diffusion. Again this may be attributed to the zero current condition requiring an increased flux of cations to compensate for the relatively rapid flow of anions. The relationship between hydrogen flux and α (for $\mathscr{C}_0 = 1$ and $\mathscr{C}_1 = 2$) is illustrated in Fig. 1(a).

After redimensionalization, Eq. (34) becomes

$$J_H = \frac{2D_H}{L(\alpha+1)}(\mathscr{B}_0 - \mathscr{B}_1) = \overline{J_H}. \tag{36}$$

This may be used to define the "effective" diffusion coefficient of hydrogen

$$D_{\text{eff}} = \frac{2D_H}{\alpha+1}. \tag{37}$$

A simple experiment measuring the ratio of flux and concentration difference would calculate the quantity D_{eff}, which is related to (but distinct from) the "actual" molecular diffusion coefficient D_H. Furthermore this calculated D_{eff} necessarily depends on the counter-ion present in the experimental preparation. This relationship is algebraically equivalent to the "Nernst-Haskell" equation which describes the combined diffusion of strong electrolyte salts. An equivalent expression has previously been reported in Ref. [15], which also examines the diffusion of hydrogen through hydrogels, although that work did not consider the effect that binding chemistry may have on ion flux.

Furthermore, in the case of $c_T = 0$, we can algebraically solve for hydrogen concentration as a function of space to get

$$h(x) = \mathscr{C}_0 + (\mathscr{C}_1 - \mathscr{C}_0)x, \tag{38}$$

which is (unsurprisingly) a linear concentration profile. Eqs. (33) and (38) may be used to evaluate the electric potential as a function of space,

$$\Psi(x) = \frac{(1-\alpha)}{(\alpha+1)} \ln\left[1 + \left(\frac{\mathscr{C}_1}{\mathscr{C}_0} - 1\right)x\right]. \tag{39}$$

Equation (39) gives the total potential difference from bath to bath

$$\Psi_1^{\text{out}} = \frac{(1-\alpha)}{(\alpha+1)} \ln\left(\frac{\mathscr{C}_1}{\mathscr{C}_0}\right). \tag{40}$$

Thus, the model gives a closed form expression for the potential difference induced across an Ussing chamberlike device as a function of the bath concentrations and the relative diffusivities of the ions used. This relationship is illustrated (for $\mathscr{C}_0 = 0$ and $\mathscr{C}_1 = 2$) in Fig. 1(b).

In the limit that the mobility of one ion through the "inner" domain is restricted we have

$$\lim_{\alpha\to\infty} \Psi_1^{\text{out}} = -\ln\left(\frac{\mathscr{C}_1}{\mathscr{C}_0}\right), \quad \text{or} \quad \lim_{\alpha\to 0} \Psi_1^{\text{out}} = \ln\left(\frac{\mathscr{C}_1}{\mathscr{C}_0}\right). \tag{41}$$

These expressions are simply the Nernst potential associated with two baths separated by a barrier impermeable to the anion and cation, respectively. Thus, the model recapitulates multiple classical results in the case that the inner layer contains no mucus.

B. With mucus

Now we investigate the behavior of the system when the background network is added to the inner domain. In this subsection, we maintain $K = 0$, but vary both c_T and α. This

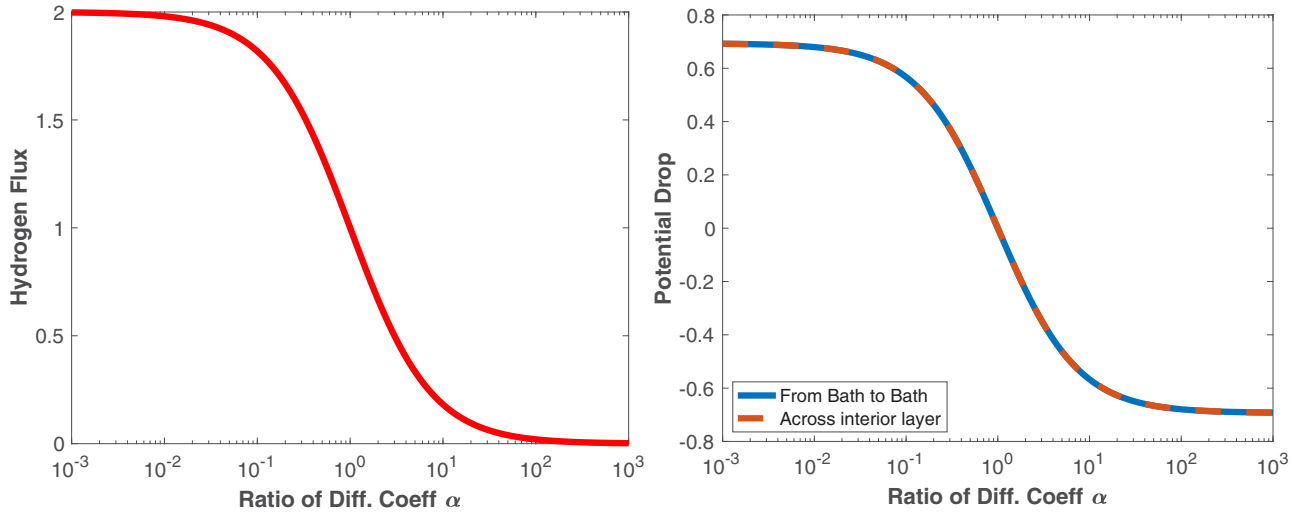

FIG. 1. The flux of hydrogen $-j_h$ vs α is shown in panel (a). For convenience, $-j_h$ is shown so that the illustrated data are positive. Purely Fickian diffusion would predict $-j_h = 1$ for the given bath concentrations. The electric potential across the interior domain ($\Psi_1^{\text{in}} - \Psi_0^{\text{in}}$) and from bath to bath (Ψ_1^{out}) are shown in panel (b). In all cases $\mathscr{E}_1 - \mathscr{E}_0 = 1$ and $K = 0$.

means that the mucus is not chemically reactive, but its electrical charge must be accounted for and will affect the diffusion of both charged species.

1. *Hydrogen flux*

Rederivation of Eq. (30) when $K = 0$ yields the expression

$$j_h = \frac{c_T(\alpha-1)}{(\alpha+1)^2}\ln\left|\frac{(\alpha+1)h_1^{\text{in}} - c_T}{(\alpha+1)h_0^{\text{in}} - c_T}\right| - \frac{2}{(\alpha+1)}\left(h_1^{\text{in}} - h_0^{\text{in}}\right). \tag{42}$$

However, in this case the inner boundary concentration is not equal to the bath concentration. When $K = 0$, the polynomial defining h_j^{in} may be solved explicitly:

$$h_j^{\text{in}} = \frac{c_T + \sqrt{c_T^2 + 4\mathscr{E}_j^2}}{2}. \tag{43}$$

Equations (42) and (43) together fully determine the flux of hydrogen as a function of model parameters. By substituting Eq. (43) into Eq. (42) and defining the imposed concentration difference $\Delta = \mathscr{E}_1 - \mathscr{E}_0 = \mathscr{E}_1 - 1$, one can arrive at an expression for the hydrogen flux as a function of Δ:

$$j_h = \frac{c_T(\alpha-1)}{(\alpha+1)^2}\ln\left|\frac{(\alpha-1)c_T + (\alpha+1)\sqrt{c_T^2+4\mathscr{E}_1^2}}{(\alpha-1)c_T + (\alpha+1)\sqrt{c_T^2+4}}\right| - \frac{1}{(\alpha+1)}\left(\sqrt{c_T^2+4\mathscr{E}_1^2} - \sqrt{c_T^2+4}\right). \tag{44}$$

In Fig. 2 we graph both the raw ($-j_h$) and normalized ($j_h/\overline{j_h}$) hydrogen flux as a function of Δ, for multiple values of c_T (with $\alpha = 1$ for simplicity). The dashed line in Fig. 2(a) indicates a linear function of Δ. From Fig. 2(b), it appears as though the normalized flux approaches a constant value in the limit of small Δ. This is indeed true, as combining Eqs. (42) and (43) and performing an asymptotic expansion in the limit $\Delta \to 0$ gives

$$j_h = \frac{-4\Delta}{c_T(\alpha-1) + (\alpha+1)\sqrt{c_T^2+4}} + \mathcal{O}(\Delta^2),$$
$$j_h/\overline{j_h} \approx \frac{2(\alpha+1)}{c_T(\alpha-1) + (\alpha+1)\sqrt{c_T^2+4}}. \tag{45}$$

Similarly, Fig. 2(b) seems to indicate that for large concentration differences, the normalized flux of hydrogen approaches unity, and the effects of mucus are negligible. Performing an expansion in the limit $\Delta \to \infty$, we see that

$$j = \frac{-2\Delta}{(\alpha+1)} + \mathcal{O}[\ln(\Delta)], \quad j_h/\overline{j_h} \approx 1. \tag{46}$$

Thus, for small concentration gradients, hydrogen flux will always be less than "expected" (assuming $\alpha > 1$) by a factor which depends relatively simply on the network charge concentration. This effect disappears as the concentration difference becomes large, and hydrogen flux approaches the "expected" rate. The distinction between "large" and "small" concentration gradients depends on the network charge concentration c_T, with more dense networks slowing hydrogen flux over a larger range of concentration gradients.

We note here that the nonlinear dependence of flux on concentration difference may go some ways to explaining the contradictory results of Refs. [6–8]. The work of Pfeiffer imposed a concentration difference (nondimensional) of $\Delta \approx 10^4$, while Williams *et al.* used a much larger gradient of $\Delta \approx 10^{5.5}$ [7,8]. It is difficult to ascertain the concentration difference analogous to the experiments of Livingston *et al.* as the smaller bath concentration $\mathscr{B}_0$ used was the ambient pH of the harvested mucus, which could reasonably vary by several orders of magnitude depending on the collection procedure. The larger hydrogen chloride concentration bath used was 150 μ M, which implies an imposed concentration difference

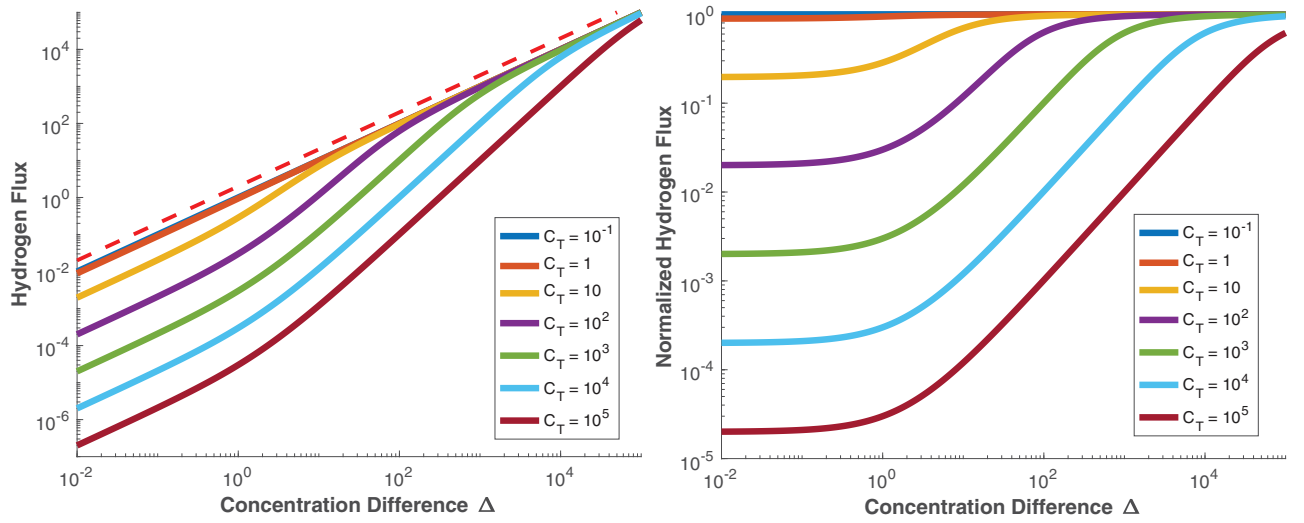

FIG. 2. The flux of hydrogen as a function of bath concentration difference (Δ). In panel (a), $-j_h$ is shown for multiple values of c_T. For convenience, $-j_h$ is shown so that the illustrated data are positive. The dashed line indicates a Δ^1 scaling law. In panel (b), the normalized flux of hydrogen $j_h/\overline{j_h}$ is shown. This may be interpreted as the ratio of hydrogen flux to "expected" hydrogen flux.

anywhere between $\Delta \approx 10^6$ and $\Delta \approx 10^3$ [8]. In all of these studies, it is difficult to estimate the charge and binding site density in the mucus preparations used, as the authors make no attempt to quantify this value. However, the work of Schreiber *et al.* suggests that the binding site density may be on the order of 100 μ M [17]. In nondimensional units this would imply a values of c_T in the range of approximately $10^{4.5}$ (Pfeiffer) to 10^6 (Williams *et al.* [8] and Livingston *et al.* [6]).

To further quantify the effect of charge density, in Fig. 3 we plot both $-j_h$ and $j_h/\overline{j_h}$ as a function of c_T, for multiple values of α (once again when $\ell_1 = 2$ and $\ell_0 = 1$). When $\alpha \geqslant 1$ (i.e., $D_H > D_C$), both measurements of hydrogen flux are monotonically decreasing functions of both c_T and α. Once again we see that decreased anion mobility (increased α) results in a reduction of hydrogen cation flux relative to the expected value. Furthermore, the presence of mucus (even in the absence of chemical binding) also reduces the flux of hydrogen; both relative to Fickian diffusion ($j_h = -1$) and electrodiffusion through an aqueous environment ($\overline{j_h}$).

In the limit of large network charge density, the dependence of hydrogen flux on mucus density is relatively simple. Combining Eqs. (42) and (43) and performing an asymptotic expansion as $c_T \to \infty$ gives the expression

$$j_h = \frac{1}{\alpha}\left(\ell_0^2 - \ell_1^2\right)c_T^{-1} + \mathcal{O}\left(c_T^{-3}\right). \tag{47}$$

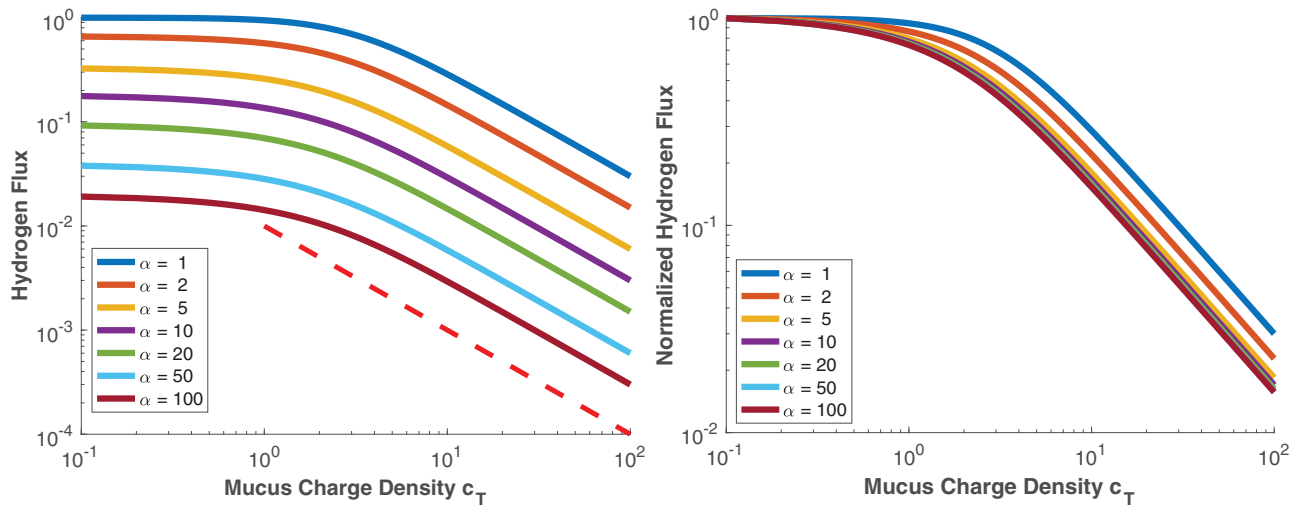

FIG. 3. The flux of hydrogen as a function of mucus charge density (c_T). In panel (a), $-j_h$ is shown for multiple values of α. For convenience, $-j_h$ is shown so that the illustrated data are positive. The dashed line indicates a c_T^{-1} scaling law. In panel (b), the normalized flux of hydrogen $j_h/\overline{j_h}$ is shown. This may be interpreted as the ratio of hydrogen flux to "expected" hydrogen flux.

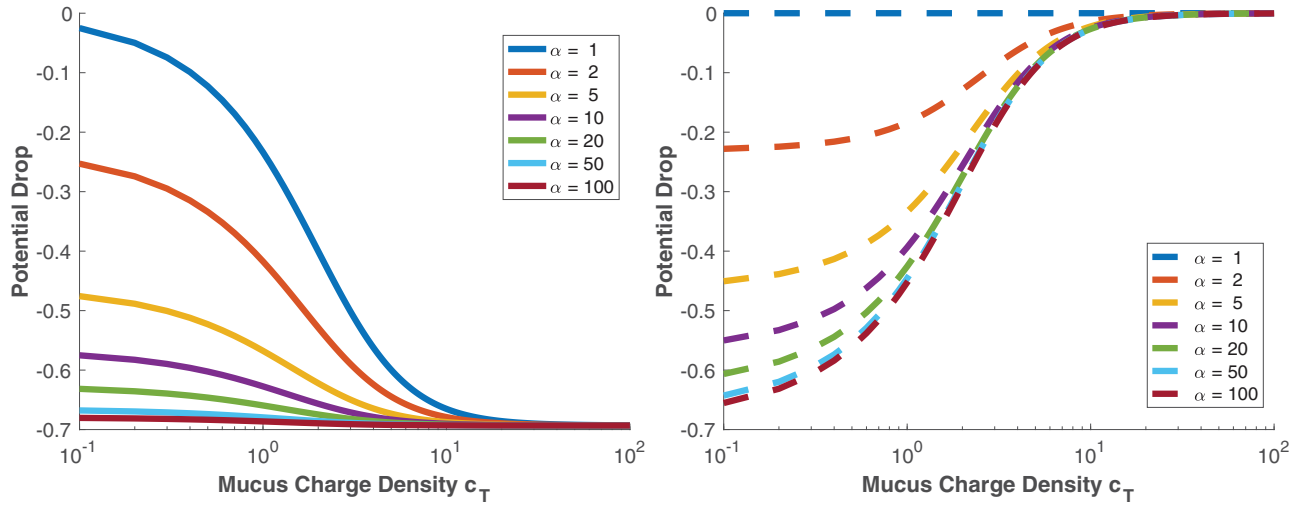

FIG. 4. The electric potential drop as a function of mucus charge density (c_T). In panel (a) Ψ_1^{out}, the total drop from bath to bath, is shown for multiple values of α. In panel (b), the drop across the interior domain ($\Psi_1^{\text{in}} - \Psi_0^{\text{in}}$) is shown.

Thus, we see that the flux of hydrogen has an inverse linear relationship with network charge density in the limit of abundant mucus. Figure 3(a) shows a reference line (dashed red) indicating a power law scaling with power -1. Furthermore, in this limit the ratio of flux to expected flux is given by

$$j_h/\overline{j_h} \approx \frac{(\alpha+1)(\mathscr{E}_0+\mathscr{E}_1)}{2\alpha c_T}, \tag{48}$$

which again scales as the inverse of network charge density, but has a much less pronounced dependence on α, as shown in Fig. 3(b). Similarly, an asymptotic expansion of Eq. 30 in the limit where the anion is much less mobile than the cation ($\alpha \to \infty$) gives

$$j_h = \left[2\left(h_0^{\text{in}} - h_1^{\text{in}}\right) + c_T \ln\left(\frac{h_1^{\text{in}}}{h_0^{\text{in}}}\right)\right]\alpha^{-1} + \mathcal{O}(\alpha^{-2}), \tag{49}$$

and thus the flux of hydrogen is also inversely proportional to α (regardless of the magnitude of c_T).

2. *Electric potential*

We now turn our attention to quantifying the potential drop (both across the inner domain, and from bath to bath). Rederivation of Eq. (28) when $K = 0$ gives the expression

$$\Psi_1^{\text{in}} - \Psi_0^{\text{in}} = \frac{\alpha-1}{\alpha+1} \ln\left|\frac{(\alpha+1)h_0^{\text{in}} - c_T}{(\alpha+1)h_1^{\text{in}} - c_T}\right|, \tag{50}$$

where h_j^{in} is still given by Eq. (43). In conjuction with Eq. (22), this expression allows us to evaluate the potential drop from bath to bath (Ψ_1^{out}). Figure 4 shows the computed potential drops as a function of c_T for various values of α. Figure 4(a) illustrates the potential of the left bath, while Fig. 4(b) illustrates the potential difference across the inner domain (again, with $\mathscr{E}_0 = 1$ and $\mathscr{E}_1 = 2$). It is immediately clear that the potential difference across the entire device is monotonically decreasing in both α and c_T. However, it appears to have a finite, nonzero limit. Conversely, the potential drop across the inner domain is an increasing function of c_T.

Equations (22), (28), and (43) may be used to show that in the limit of large c_T,

$$\Psi_1^{\text{in}} - \Psi_0^{\text{in}} = \frac{(\alpha-1)\left(\mathscr{E}_0^2 - \mathscr{E}_1^2\right)}{\alpha} c_T^{-2} + \mathcal{O}\left(c_T^{-3}\right), \tag{51}$$

$$\Psi_1^{\text{out}} = -\ln\left(\frac{\mathscr{E}_1}{\mathscr{E}_0}\right) + \frac{\mathscr{E}_1^2 - \mathscr{E}_0^2}{\alpha} c_T^{-2} + \mathcal{O}\left(c_T^{-4}\right). \tag{52}$$

Thus, as the background network charge becomes more dense, the potential drop across the inner domain approaches zero. Furthermore, Eq. (22) guarantees that in this limit, the ion concentrations at both boundaries are equal (to c_T), which implies that there is no electrochemical potential driving a flux of hydrogen through the inner domain. This provides a physical explanation for the behavior illustrated in Fig. 3. We also note that Eq. (52) implies that as the network charge density increases, we recover the Nernst potential, as an infinite density of negative charge within the layer makes it impermeable to the anion. A similar expansion may be performed in the limit of large α to yield

$$\Psi_1^{\text{in}} - \Psi_0^{\text{in}} = -\ln\left(\frac{h_1^{\text{in}}}{h_0^{\text{in}}}\right) + \mathcal{O}\left(\alpha^{-1}\right), \tag{53}$$

$$\Psi_1^{\text{out}} = -\ln\left(\frac{\mathscr{E}_1}{\mathscr{E}_0}\right) + \mathcal{O}\left(\alpha^{-1}\right), \tag{54}$$

where the inner concentrations are still given by Eq. (43). Thus, the potential difference across the inner domain approaches a nonzero value determined by the background charge density c_T. However, the potential difference from bath to bath recovers the Nernst potential of an immobile anion, and we see that the prediction of Eq. (41) holds even in the presence of mucus.

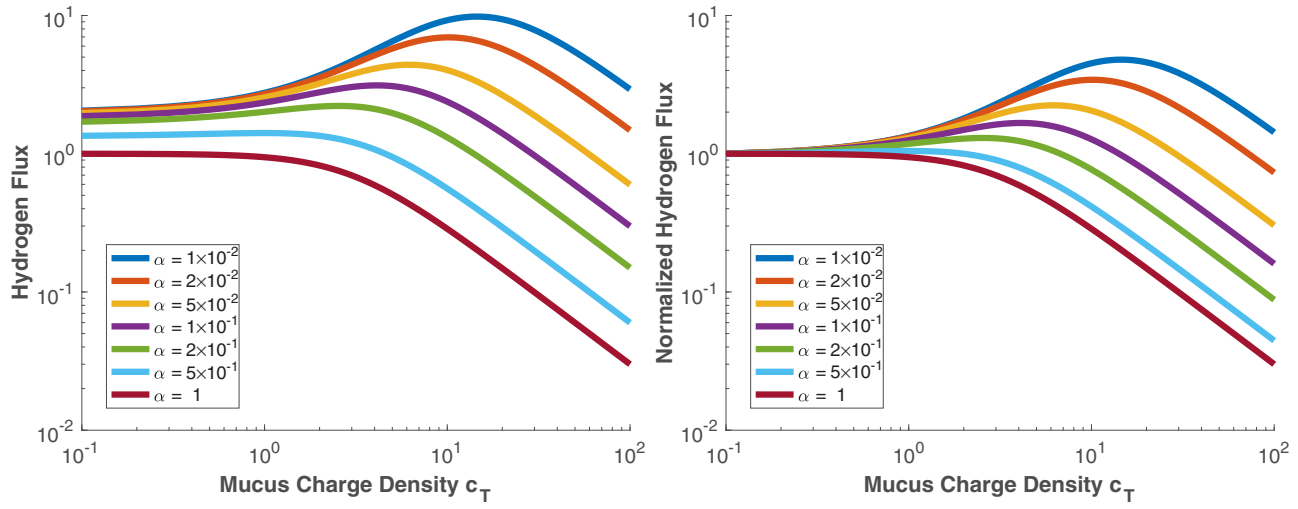

FIG. 5. The flux of hydrogen as a function of mucus charge density (c_T). In panel (a), $-j_h$ is shown for multiple values of $\alpha \leqslant 1$. For convenience, $-j_h$ is shown so that the illustrated data are positive. In panel (b), the normalized flux of hydrogen $j_h/\overline{j_h}$ is shown. This may be interpreted as the ratio of hydrogen flux to "expected" hydrogen flux.

C. With a more mobile anion

Thus far we have restricted our analysis to the case that $\alpha \geqslant 1$ ($D_H \geqslant D_C$), as our motivation is the characterization of hydrogen flux through a mucus network, and hydrogen has the greater mobility in any hydrogen halide. However, the same modeling framework may be used to describe the diffusive transport of any cation-anion pair. When still restricted to the case that $K = 0$, Eqs. (42), (43), and (50) still hold, but lead to a different characterization of cation flux. Figure 5 shows the calculated values of $-j_h$ and $j_h/\overline{j_h}$ as a function of c_T, for various values of α. Again, in the limit of high network charge density we still see the same c_T^{-1} power law scaling. However, flux is no longer a monotonic function of c_T. A series representation of Eqs. (42) and (43) in the limit $\alpha \to 0$ yields

$$j_h = -\left(\sqrt{c_T^2 + 4\mathscr{O}_1^2} - \sqrt{c_T^2 + 4\mathscr{O}_0^2}\right) - c_T \ln\left(\frac{c_T - \sqrt{c_T^2 + 4\mathscr{O}_1^2}}{c_T - \sqrt{c_T^2 + 4\mathscr{O}_0^2}}\right) + \mathcal{O}(\alpha), \tag{55}$$

which has a local maximum at finite $c_T > 0$.

It appears that the nonmonotonicity of cation flux may be attributed to the electric potential gradient induced across the inner domain in the case of small α. Figure 6 shows the total and inner potential drops as a function of c_T, for multiple values of $\alpha \leqslant 1$. Expansion of Eqs. (50) and (22) in this limit yields

$$\Psi_1^{\text{in}} - \Psi_0^{\text{in}} = \ln\left(\frac{c_T - \sqrt{c_T^2 + 4\mathscr{O}_1^2}}{c_T - \sqrt{c_T^2 + 4\mathscr{O}_0^2}}\right) + \mathcal{O}(\alpha), \tag{56}$$

$$\Psi_1^{\text{out}} = \ln\left(\frac{\mathscr{O}_1}{\mathscr{O}_0}\right) + \mathcal{O}(\alpha). \tag{57}$$

Thus, while the potential drop from bath to bath approaches a constant (the Nernst potential for a domain impermeable to the cation), the potential drop across the inner domain is a nonmonotonic function of network charge density. This in turn implies that the electrochemical potential gradient driving the flux of ions across the layer has a nontrivial dependence on mucus charge density, leading to the flux behavior shown in Fig. 5.

D. Nonzero K

Now, we address the case when $K \neq 0$. In this case, the expressions defining j_h, and Ψ_1^{out} are more complex, depend on more parameters, and can not be as easily analyzed quantitatively. However, graphical analysis indicates that the behavior is qualitatively similar to that outlined in previous sections. Figure 7 shows the flux of hydrogen ($-j_h$), as well as the potential drop from bath to bath (Ψ_1^{out}) as a function of the mucus charge concentration (c_T) and hydrogen/mucus association constant (K). The data shown in Fig. 7 were generated with $\mathscr{O}_0 = 1$, $\mathscr{O}_1 = 2$ (as in previous sections) and $\alpha = 1$ (as a point of reference). In this case, $\overline{j_h} = -1$ and therefore the flux of hydrogen and the normalized flux of hydrogen are equivalent. The solid and dashed red level curves shown in Fig. 7(a) indicate $-j_h = 0.75$ and $-j_h = 0.25$, respectively. The region between these level curves corresponds with hydrogen diffusion through the layer that is slowed by 25–75%, which is consistent with some experimental studies [6–8]. The same level curves are reproduced in Fig. 7(b) to indicate the approximate range of potential drops (from bath to bath) that are consistent with diffusion slowed by this amount. We note that, generically, hydrogen flux is a decreasing function of c_T (as in previous sections) and an increasing function of K. This is very much in agreement with the analysis of Ref. [19], where it was shown that the predominant effect of binding affinity was to neutralize the background charge

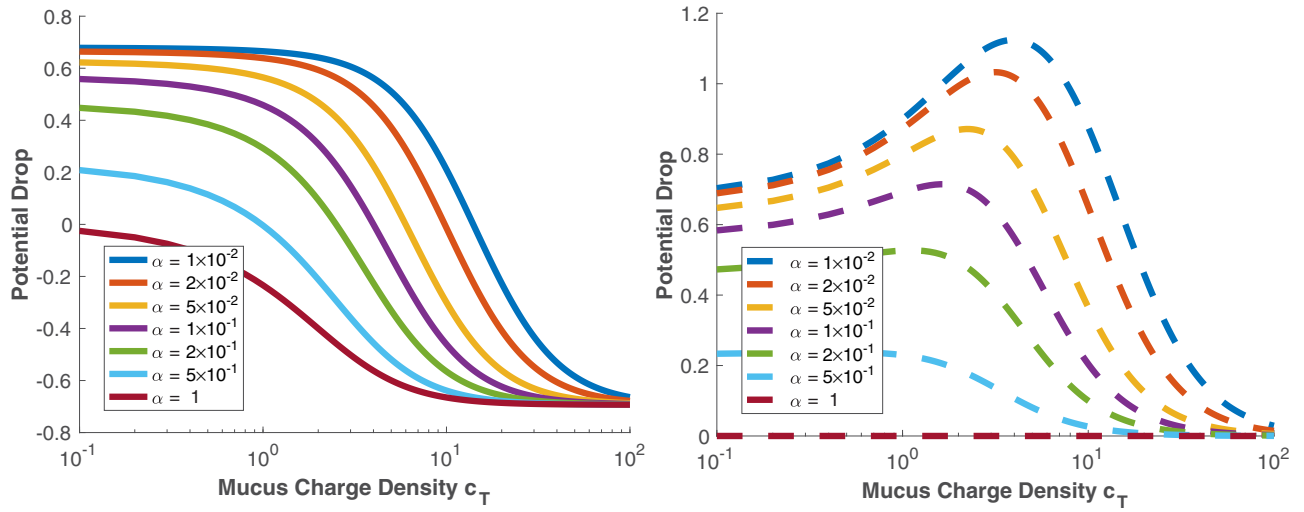

FIG. 6. The electric potential drop as a function of mucus charge density (c_T). In panel (a) Ψ_1^{out}, the total drop from bath to bath, is shown for multiple values of α. In panel (b), the drop across the interior domain ($\Psi_1^{\text{in}} - \Psi_0^{\text{in}}$) is shown.

via bound hydrogen. That is, high network charge density with high binding affinity is approximately equivalent to low network charge density with no binding affinity. This is also in agreement with the work of Marczynski *et al.* which indicated that the ability to form bonds with the network can enhance diffusive transport [9].

For comparison, and to more accurately represent the differing diffusivities of hydrogen and chloride, Fig. 8 shows the corresponding data when $\alpha = 5$. However, in this case the flux of hydrogen ($-j_h$) and the normalized flux ($j_h/\overline{j_h}$) are not equivalent, and are thus shown in Figs. 8(a) and 8(b), respectively. We note that *at most*, hydrogen flux is one third of what its *molecular* diffusion coefficient (D_H) would predict. These values are seen in the regime of small c_T (very little background charge) and large K (background charge is almost completely neutralized by bound hydrogen) and are thus purely due to the less mobile anion. However, these values are precisely what the effective diffusion coefficient (D_{eff}) would predict. Upon normalization by the expected flux ($\overline{j_h}$), the flux of hydrogen and electric potential drops [Figs. 8(b) and 8(c)] are very similar to their counterparts in Fig. 7, with two major exceptions. The potential drop across the domain is generically greater in magnitude, which must be true to maintain zero current in the presence of more mobile cation. Also, the relevant level curves of normalized flux have shifted to the left, meaning that in general, the same background charge

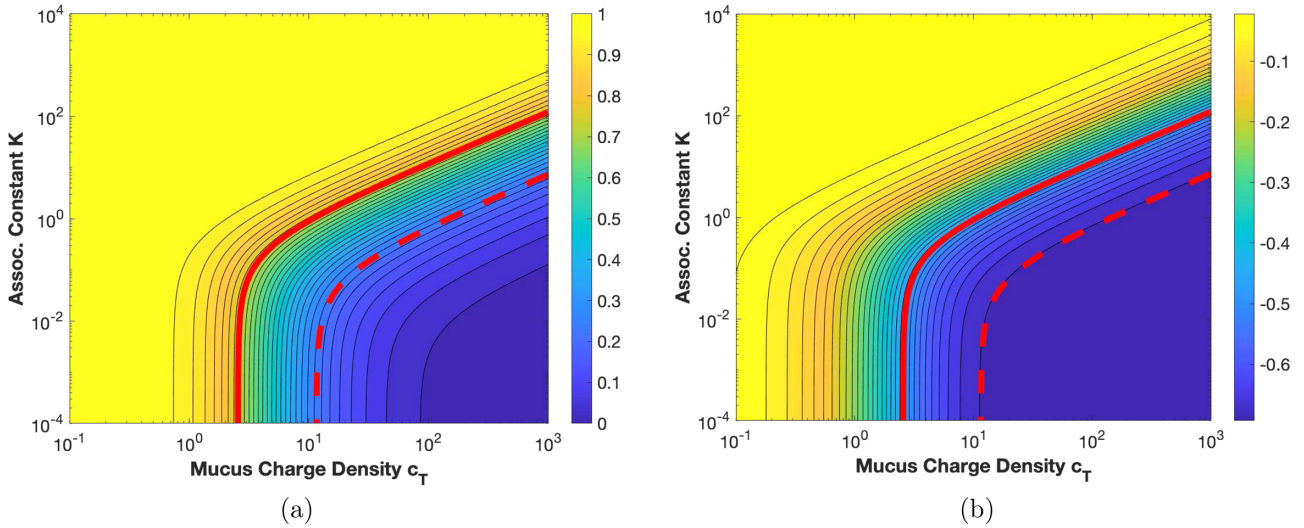

FIG. 7. Flux of hydrogen (a) and total potential drop (b) as a function of mucus charge density (c_T) and binding affinity (K). The bold solid and dashed curves indicate the $-j_h = 0.75$ and $-j_h = 0.25$ level curves, respectively. All data were generated with $\ell_1 = 2$ and $\alpha = 1$.

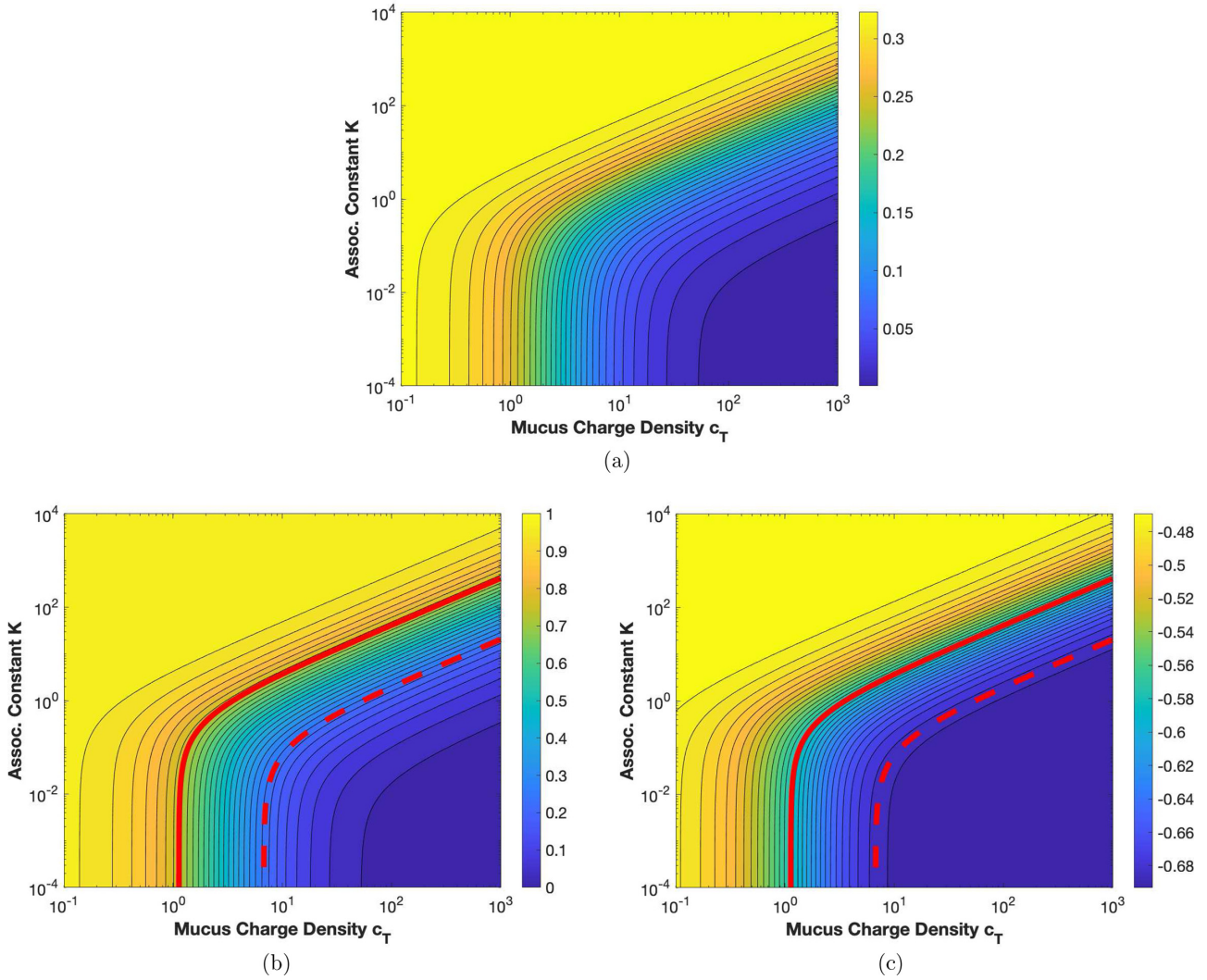

FIG. 8. Flux of hydrogen (a), normalized flux of hydrogen (b), and total potential drop (c) as a function of mucus charge density (c_T) and binding affinity (K). The bold solid and dashed curves indicate the $j_h/\overline{j_h} = 0.75$ and $j_h/\overline{j_h} = 0.25$ level curves, respectively. All data were generated with $\ell_1 = 2$ and $\alpha = 5$.

results in a smaller normalized flux of hydrogen. These trends are all in agreement with the analysis presented in previous sections.

E. Realistic parameters

We now examine the behavior of the model in a parameter regime which corresponds to experimental conditions used in the extant literature. Determining α is, in general, rather difficult, as determining the "actual" molecular diffusion coefficients of isolated ions can not be accomplished by measuring the flux of a single charged species between two known bath concentrations. However, in Ref. [15], the authors measure D_{eff} for *sodium chloride* in an aqueous environment, and then separately measure D_{Na} via a technique based on PFGSE-NMR spectroscopy. This allows the calculation of D_C via the Nernst-Haskell equation. In a second experiment, the authors then measure D_{eff} for hydrogen chloride in aqueous solution, which finally allows calculation of D_H. The values listed are summarized in Table I. The density of potential hydrogen binding sites in guinea pig gastric mucus has been measured experimentally and found to be approximately $C_T \approx 130$ mM [17]. For bath concentrations, we use the values reported in the "flux chamber" experiments of Pfeiffer [7], which are $\mathscr{B}_0 = 10^{-5.5}$ M and $\mathscr{B}_1 = 10^{-0.9}$ M. Finally, estimates of the binding affinity $\mathscr{K}(= k_+/k_-)$ based on experimental studies are difficult to find. However, in a theoretical study the authors of Ref. [25] determine $\mathscr{K} \approx 10^{-3.65}$ M^{-1} by fitting exponential swelling curves of a polyelectrolyle gel model of mucus to experimental data. These values are summarized in Table II.

TABLE I. Estimated diffusion coefficients from Ref. [15].

Quantity	Symbol	Value
Effective diffusion coefficient of HCl	D_{eff}	3.141×10^{-5} cm^2/s
Molecular diffusion coefficient of H^+	D_H	6.22×10^{-5} cm^2/s
Molecular diffusion coefficient of Cl^-	D_C	2.10×10^{-5} cm^2/s
Ratio of diffusion coefficients	α	2.96 [-]

TABLE II. Estimated chemical and bath parameters.

Quantity	Symbol	Value
Binding affinity of hydrogen	$\mathscr{K}$	$10^{-3.65}$ M^{-1}
Concentration of binding sites in Mucus	C_T	0.13 M
Temperature	T	300 K
HCL concentration in left bath	$\mathscr{B}_0$	$10^{-5.5}$ M
HCL concentration in right bath	$\mathscr{B}_1$	$10^{-0.9}$ M

To present electric potential values in dimensional units, we define

$$\Phi = \frac{RT}{F}\Psi^1_{\text{out}},$$

the potential drop across the device measured in units of mV. Model results using estimated parameters (except for $\mathscr{K}$ and C_T) are plotted as a function of both $\mathscr{K}$ and C_T in Fig. 9. Once again, we have highlighted in red the level curves which correspond to a normalized flux of hydrogen 25%–75% of the expected value. We have also added a marker (white "X") indicating the values of C_T and $\mathscr{K}$ corresponding to estimates in Table II. This marker falls between the two highlighted level curves, indicating that model predictions are well within the range consistent with experimental studies. For reference, these parameter values give rise to a normalized flux of approximately 46% and a potential drop of slightly less than 300 mV:

$$j_h/\overline{j_h} = 0.461, \quad \Phi = -269\ \text{mV}.$$

The estimate of hydrogen flux is well within the ranges reported in experimental studies, and the potential drop (while large) is well within ranges seen in many biological gel and membrane systems. For reference, we show the computed spatial profiles of all variables (ions, unbound mucus, and electric potential) in Fig. 10. As required by the Donnan equilibrium, the free hydrogen concentration immediately within the mucus layer is generically greater than the bath. This is attenuated (slightly) by hydrogen bound to the background network. The electric potential varies somewhat within the mucus layer, but this variation is drastically smaller than the potential difference induced by the Donnan equilibrium.

Finally, we note that in the estimated parameter regime, our results are *extremely* insensitive to the association constant $\mathscr{K}$. This is illustrated by the level curves on Fig. 9 in the vicinity of the "X," which are nearly vertical. The estimate of $\mathscr{K}$ obtained from Ref. [25] is the result of fitting a relatively complex model with a large number of parameters, and is therefore in some sense the parameter of "least confidence" discussed here. While we know of no other estimate for the binding affinity of hydrogen with mucus, Crowther *et al.* have measured the affinity of mucus with other, larger cations [16]. Their results indicate the following: mucus exhibits multiple different cation binding sites with different binding affinities, binding affinity is generally an increasing function of valence (with monovalent ions exhibiting the smallest binding affinity), and the ions considered all exhibited binding affinities four to six orders of magnitude larger than the $\mathscr{K}$ reported in Ref. [25]. In light of this, it may not be strictly accurate to define a *single* affinity for hydrogen and mucus binding, and the value used here may be a low estimate. However, Fig. 9 indicates that increasing our estimate of $\mathscr{K}$ by four or five orders of magnitude (comparable with the values for monovalent ions reported in Ref. [16]) would not appreciably change the model predictions.

IV. DISCUSSION

In this work we have analyzed a relatively simple, two ion model of diffusive transport through a charged mucus-like gel layer accounting for the Donnan potential associated with the gel/bath interface. In particular, we have quantified the steady-state flux of hydrogen ions through the layer and the resulting electric potential across the layer as functions of the parameters describing the electrochemical nature of the gel and the dissolved cation-anion pair. In multiple limiting

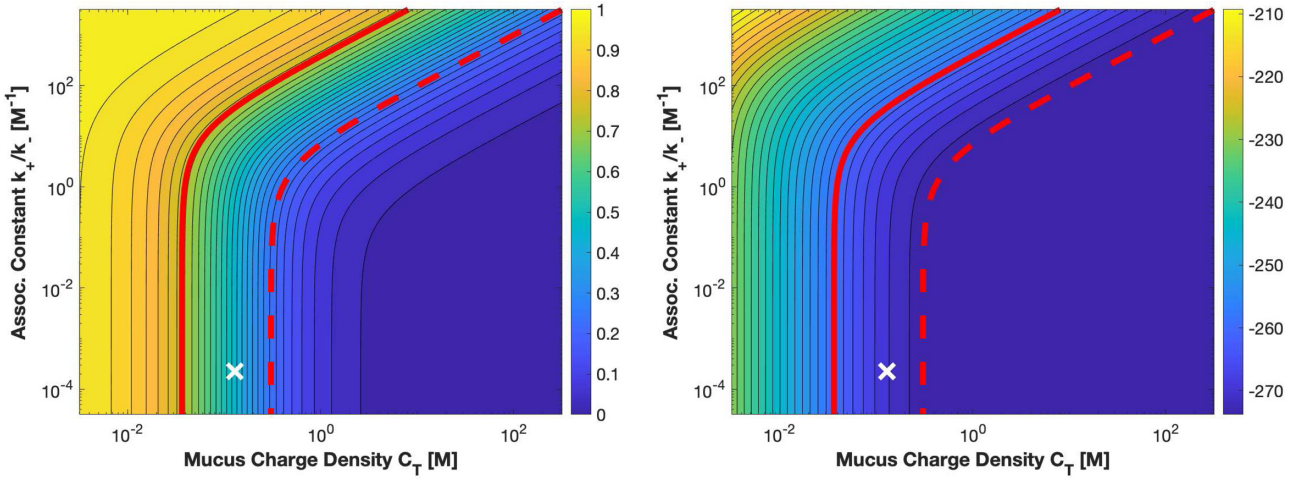

(a) (b)

FIG. 9. Normalized flux of hydrogen (a) and total potential drop (b) as a function of mucus charge density (C_T) and binding affinity ($\mathscr{K}$). The bold solid and dashed curves indicate the $j_h/\overline{j_h} = 0.75$ and $j_h/\overline{j_h} = 0.25$ level curves, respectively. All data generated with $\mathscr{B}_0 = 10^{-5.5}$ M, $\mathscr{B}_1 = 10^{-0.9}$ M, and $\alpha = 2.96$. The "X" represents the values of C_T and $\mathscr{K}$ estimated from literature.

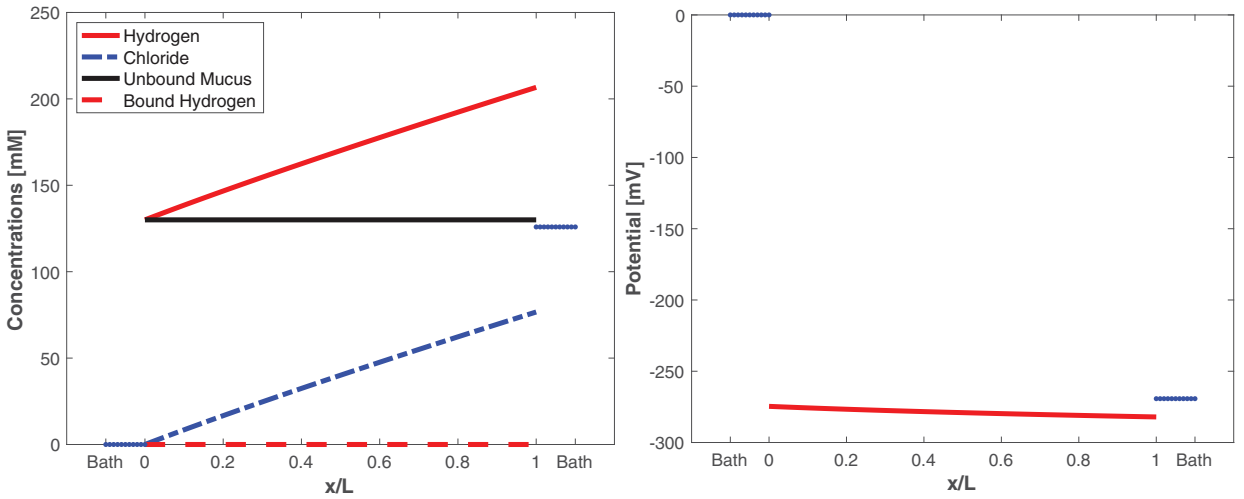

FIG. 10. Spatial profiles of the model variables for parameter values indicated by "X" in Fig. 9. In panel (a), the concentrations of free hydrogen, chloride, unbound mucus, and bound hydrogen are shown in mM. In panel (b), the electric potential Φ is shown in mV. In both panels, the bath concentrations and potentials are indicated with dotted lines.

cases, the model recapitulates classical phenomena, including the Nernst Potential associated with a semipermeable membrane across which only one ion may travel. Furthermore, we have compared the calculated flux of hydrogen to the "expected" flux in the case where the layer is devoid of mucus (no charge and/or binding sites). This was done specifically to address apparent discrepancies within the experimental literature that report multiple values of the apparent "slowdown" of hydrogen diffusion through mucus. Critically, diffusive flux of hydrogen is proportional not to the difference in bath concentrations, but to the difference in *a nonlinear function of bath concentrations* [Eq. (30)]. This implies that different experimental preparations will not only result in altered hydrogen flux, but altered hydrogen flux *relative to the expected value*. We believe this may be responsible for the variety of values present in experimental studies.

Generically, our results indicate that hydrogen flux (both gross, and relative to "expected") are decreasing functions of the charge density of the mucus, and the ratio of hydrogen ion to anion mobility. Thus, increasing mucus charge density, or using bath solutions of an anion larger than chloride will hinder hydrogen diffusion. Conversely, increased hydrogen and mucus binding affinity generically increases the flux of hydrogen. This contradicts older hypotheses in the physiological literature which suggest binding to the network may slow diffusion of hydrogen through the gastric mucus lining [26]. However, this result is very much in line with previous theoretical studies that indicate diffusion through mucus layers is largely governed by the Donnan potential at the gel layer, and the primary effect hydrogen and mucus binding is to lower the charge density of the mucus network, thus removing an impediment to electrodiffusive transport [19].

ACKNOWLEDGMENTS

The work of O. Lewis and J. Keener was partially supported by NIH Grant No. 1R01GM131408. The work of J. Keener was partially supported by NSF Grant No. DMS-1515130.

[1] R. A. Cone, Adv. Drug Delivery Rev. **61**, 75 (2009).
[2] J. Witten, T. Samad, and K. Ribbeck, Curr. Opin. Biotechnol. **52**, 124 (2018).
[3] J. D. Kaunitz, Keio J. Med. **48**, 63 (1999).
[4] J. M. Newby, I. Seim, M. Lysy, Y. Ling, J. Huckaby, S. K. Lai, and M. G. Forest, Adv. Drug Delivery Rev. **124**, 64 (2018).
[5] N. G. Heatley, Gastroenterology **37**, 313 (1959).
[6] E. H. Livingston and E. Engel, J. Clin. Gastroenterol. **21**, S120 (1995).
[7] C. J. Pfeiffer, Am. J. Physiol. **240**, G176 (1981).
[8] S. E. Williams and L. A. Turnberg, Gastroenterology **79**, 299 (1980).
[9] M. Marczynski, B. T. Käsdorf, B. Altaner, A. Wenzler, U. Gerland, and O. Lieleg, Biomater. Sci. **6**, 3373 (2018).
[10] J. S. Mackie and P. Meares, Proc. R. Soc. London A **232**, 498 (1955).
[11] P. E. Grimshaw, J. H. Nussbaum, A. J. Grodzinsky, and M. L. Yarmush, J. Chem. Phys. **93**, 4462 (1998).
[12] L. Johansson, U. Skantze, and J.-E. Loefroth, J. Phys. Chem. **97**, 9817 (1993).
[13] R. Schlögl and F. Helfferich, J. Chem. Phys. **26**, 5 (1957).
[14] F. Helfferich and M. S. Plesset, J. Chem. Phys. **28**, 418 (1958).
[15] G. Schuszter, T. Gehér-Herczegh, Á. Szűcs, A. Toth, and D. Horváth, Phys. Chem. Chem. Phys. **19**, 12136 (2017).
[16] R. S. Crowther and C. Marriott, J. Pharm. Pharmacol. **36**, 21 (1983).
[17] S. S. Schreiber and P. P. Scheid, Am. J. Physiol. **272**, G63 (1997).

[18] P. Y. Tam and P. Verdugo, Nature (London) **292**, 340 (1981).
[19] O. L. Lewis and J. P. Keener, SIAM J. Appl. Math. **81**, 965 (2021).
[20] P. Verdugo, I. Deyrup-Olsen, A. W. Martin, and D. L. Luchtel, in *Mechanics of Swelling: From Clays to Living Cells and Tissues* (Springer-Verlag, Berlin, 1992), pp. 671–681.
[21] W. Hong, X. Zhao, and Z. Suo, J. Mech. Phys. Solids **58**, 558 (2010).
[22] S. Sircar, J. P. Keener, and A. L. Fogelson, J. Chem. Phys. **138**, 014901 (2013).
[23] Y. Yu, C. M. Landis, and R. Huang, J. Appl. Mech. **84**, 051005 (2017).
[24] See Supplemental Material at http://link.aps.org/supplemental/10.1103/PhysRevE.104.044403 for a complete description of the calculations to solve model equations.
[25] S. Sircar and A. Roberts, Discrete Contin. Dyn. Syst. Ser. B **21**, 1937 (2016).
[26] A. Allen and G. Flemström, Am. J. Physiol. Cell Physiol. **288**, C1 (2005).